JACS
JOURNAL OF THE AMERICAN CHEMICAL SOCIETY

Communication

pubs.acs.org/JACS

Synthesis of High-Quality Brookite TiO_2 Single-Crystalline Nanosheets with Specific Facets Exposed: Tuning Catalysts from Inert to Highly Reactive

Haifeng Lin,[†] Liping Li,[†] Minglei Zhao,[†] Xinsong Huang,[‡] Xiaomei Chen,[†] Guangshe Li,*[,†] and Richeng Yu[§]

[†]State Key Laboratory of Structural Chemistry, Fujian Institute of Research on the Structure of Matter, Chinese Academy of Sciences, Fuzhou 350002, P. R. China

[‡]Key Laboratory of Coal to Ethylene Glycol and Its Related Technology, Chinese Academy of Sciences, Fuzhou 350002, P. R. China

[§]Beijing National Laboratory of Condensed Matter Physics, Institute of Physics, Chinese Academy of Sciences, Beijing 100190, P. R. China

Supporting Information

ABSTRACT: The brookite phase of TiO_2 is hardly prepared and rarely studied in comparison with the common anatase and rutile phases. In addition, there exist immense controversies over the cognition of the light-induced liveliness of this material. Here, a novel, low-basicity solution chemistry method was first used to prepare homogeneous high-quality brookite TiO_2 single-crystalline nanosheets surrounded with four {210}, two {101}, and two {201} facets. These nanosheets exhibited outstanding activity toward the catalytic degradation of organic contaminants superior even to that of Degussa P25, due to the exposure of high-energy facets and the effective suppression of recombination rates of photogenerated electrons and holes by these facets as the oxidative and reductive sites. In contrast, irregularly faceted phase-pure brookite nanoflowers and nanospindles were inactive in catalytic reactions. These results demonstrate that the photocatalytic activity of brookite TiO_2 is highly dependent upon its exposed facets, which offers a strategy for tuning the catalysts from inert to highly active through tailoring of the morphology and surface structure.

Titanium dioxide is regarded as one of the most promising materials and has played an increasingly important role in the remission of environmental and energy crises in recent years.[1,2] Among the three main crystallographic forms of TiO_2, naturally metastable brookite is the least investigated in comparison with the comprehensively studied anatase and rutile phases because of the difficulties encountered in acquiring its pure form.[3] What is more, selective control over the exposure of specific crystal faces, especially the higher-energy facets of brookite, seems even harder in this respect.

In the catalytic area, cognition of the photocatalytic activity of brookite TiO_2 is highly controversial: some reports indicate that brookite is inactive toward degradation of dyes,[4] while others conclude that brookite is more reactive than its counterparts anatase and rutile in terms of unit specific surface area.[5,6] Over this issue, the synergy in the frequently anatase- and rutile-contaminated brookite TiO_2 enhances the photocatalytic activity, which to some extent might confuse people about the origin of the activity.[4] On the other hand, reactive or high-energy facets in catalysts contribute significantly to their excellent activities in catalytic reactions.[7,8] To settle the disputes and interpret how to heighten their catalytic performances, we synthesized three forms of high-quality brookite TiO_2 single crystals, namely, uniform nanospindles, nanoflowers, and nanosheets, using a novel solution chemistry approach. Morphology characterizations showed that both the nanospindles and nanoflowers were irregularly faceted, while the nanosheets were bounded by well-defined {210}, {101}, and {201} facets. The catalytic activities of these three distinct morphologies were evaluated by using light-catalyzed degradation of dyes as a probe reaction. It was found that both nanospindles and nanoflowers were inert toward bleaching of dyes. Surprisingly, brookite nanosheets possessing a similar specific surface area and absorption edge as the nanospindles were extraordinarily active in degradation reactions, superior even to Degussa P25 TiO_2, as a consequence of the presence of the high-energy {101} facets and efficient suppression of photoinduced electron−hole pair recombination by these unfolded facets as the oxidative and reductive sites.[9] Therefore, the catalytic activity of phase-pure brookite TiO_2 is highly dependent upon its specific exposed facets. These results demonstrate that one can tune any catalyst from inert to highly reactive simply by means of exposing some designated facets.

High-quality brookite TiO_2 nanosheets were prepared through a low-basicity hydrothermal process utilizing $TiCl_4$ as a titanium source, urea as an in situ OH^- source, and sodium lactate as the complexant and surfactant. After reaction at 200 °C for 12 h, the product was phase-pure brookite TiO_2, as indicated by the X-ray diffraction (XRD) pattern in Figure 1a. Transmission electron microscopy (TEM) observations showed that the product consisted of a large number of small nanosheets with a regularly truncated tetragonal shape (Figure 1b). High-resolution TEM (HRTEM) indicated the single-

Received: February 12, 2012
Published: May 4, 2012

ACS Publications © 2012 American Chemical Society

dx.doi.org/10.1021/ja3014049 | J. Am. Chem. Soc. 2012, 134, 8328−8331

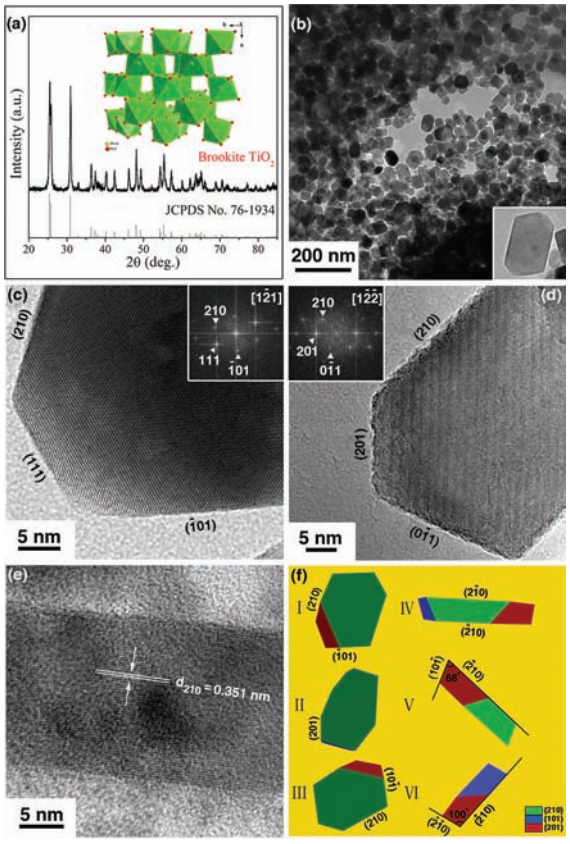

Figure 1. (a) Typical XRD pattern and (b) low-magnification TEM image of phase-pure brookite nanosheets prepared after reaction at 200 °C for 12 h. (c–e) HRTEM images and (insets) corresponding FFT results for (c, d) horizontally and (e) vertically oriented nanosheets. (f) Views of the nanosheet model in various orientations ({210}, {101}, and {201} facets are represented in green, blue, and red, respectively).

crystalline nature of the nanosheets, which had a length of ~80 nm, a width of ~60 nm, and a thickness of ~15 nm.

On the basis of the fast Fourier transform (FFT) analysis of the lattice fringes (Figure 1c), it can be concluded that the brookite nanosheets are surrounded with facets parallel to the sharply terminated (210), $(\bar{2}10)$, $(10\bar{1})$, $(\bar{1}01)$, (111), and $(\bar{1}\bar{1}1)$ edges (incident beam parallel to $[1\bar{2}1]$). Careful examinations of the lattice fringes of single nanosheets indicated that the contrast is alike in the areas close to two {210} and two {101} boundaries, which is apparently higher than that for {111} ones. Hence, four borders (i.e., two {210} and two {101} boundaries) shape the side facets of each nanosheet, while the other edges like (111) and $(\bar{1}\bar{1}1)$ do not [also see Figure S4a in the Supporting Information (SI)]. When the sample holder was tilted to render the nanosheet to be $[1\bar{2}\bar{2}]$ oriented (Figure 1d), the lattice fringes were observed to terminate sharply at (201) and $(\bar{2}0\bar{1})$ boundaries, indicating that these edges form the facets of the nanosheet surface. In addition, the spacing of the fringes parallel to the top and bottom of the vertical nanosheet was 0.351 nm (Figure 1e), which can be attributed to the $(2\bar{1}0)$ and $(\bar{2}10)$ facets of brookite TiO_2. Further observations on various erected nanosheets revealed angles of ~68° between the exposed $(\bar{2}10)$ and $(10\bar{1})$ planes and ~100° between the $(\bar{2}10)$ and $(2\bar{1}0)$ facets (Figure S4b,d), which agree well with the theoretical angles of 68.05° and 99.82°, respectively. Therefore, each nanosheet is surrounded by four {210}, two {101}, and two {201} facets. With these analyses, a stereo-shape model was constructed (see Figure 3d). Projections obtained by rotating this model were in complete accordance with the appearances that we observed experimentally. For instance, case I in Figure 1f corresponds to Figure 1c, while cases II–VI match well with Figures 1d, S4a, 1e, S4b, and S4d, respectively.

As indicated by Raman spectra [Figure S5(II)], samples of nanosheets, nanospindles, and nanoflowers showed high phase purity of the brookite structure. Additional scanning electron microscopy (SEM) and HRTEM observations on both nanospindles and nanoflowers indicated a single-crystal structure of brookite but with no particular facets exposed (Figure S5). Furthermore, regardless of morphology, similar brookite absorption edges and band-gap energies were observed. As manifested by UV–vis diffuse reflectance spectra (Figure S6a), the absorption edges were found to be 389.1, 386.3, and 382.6 nm for the nanoflowers, nanospindles, and nanosheets, respectively. The corresponding band-gap energies were 3.03, 3.05, and 3.13 eV, as determined from plots of $(Ah\nu)^{1/2}$ versus energy $(h\nu)$ (Figure S6b);[5] these all fall between the values of ~3.2 eV for anatase and 3.0 eV for rutile[5,10] but are smaller than that of 3.4 eV for granular brookite nanoparticles reported elsewhere.[11,12]

The formation of brookite nanoflowers and nanospindles might proceed through the decomposition of titanates, as previously reported.[6,13] Recently, a few water-soluble titanium-containing organic complexes have been explored as precursors in the synthesis of phase-pure brookite TiO_2,[14,15] although the precursor preparation is cumbersome and the resulting grains are usually irregularly faceted. Herein we initially adopted a novel in situ-generated precursor, $[Ti(C_3H_4O_3)_3]^{2-}$, for the formation of phase-pure brookite. This precursor (chiral space group $P2_13$)[16] is more asymmetric than the commercial TALH complex used for brookite synthesis by Bahnemann and co-workers.[15] Since brookite is featured by its low symmetry, our $[Ti(C_3H_4O_3)_3]^{2-}$ complex could be more efficient in forming the brookite architecture under mild conditions such as a much lower urea concentration and a shorter preparation period. The preparation conditions were further optimized by a collection of contrast experiments (Figures S2, S10, S11, and S12) and sample characterizations (Figures S2 and S3). When the $TiCl_4$ starting material was dissolved in water, the water-soluble complex $[Ti(OH)_2(OH_2)_4]^{2+}$ could be initially formed, and the reaction solution became strongly acidic.[17,18] This complex may then be transformed into the brookite precursor $[Ti(C_3H_4O_3)_3]^{2-}$ upon addition of sodium lactate to the reaction solution. Considering the roles of lactate ions in forming the $[Ti(C_3H_4O_3)_3]^{2-}$ complex as reported in the literature,[14,16] the formation process for the current brookite precursor can be expressed as follows:

$$TiCl_4 + 6H_2O \rightarrow [Ti(OH)_2(OH_2)]^{2+} + 2H^+ + 4Cl^-$$

$$[Ti(OH)_2(OH_2)_4]^{2+} + 3C_3H_4O_3{}^{2-} \rightarrow [Ti(C_3H_4O_3)_3]^{2-} + 2OH^- + 4H_2O$$

Such a precursor could not be transformed into the brookite lattice but instead gave anatase when urea was incompletely dissociated within the first 2 h of hydrothermal reaction at pH <8 (Figure S2). When the reaction period was prolonged from 2 to 12 h, the urea was completely disintegrated to create a moderately alkaline solution (i.e., pH 8–9), and the precursor

dx.doi.org/10.1021/ja3014049 | J. Am. Chem. Soc. 2012, 134, 8328–8331

was entirely condensed to form brookite through oxolation during the crystallization process (Figure 2). Meanwhile, the

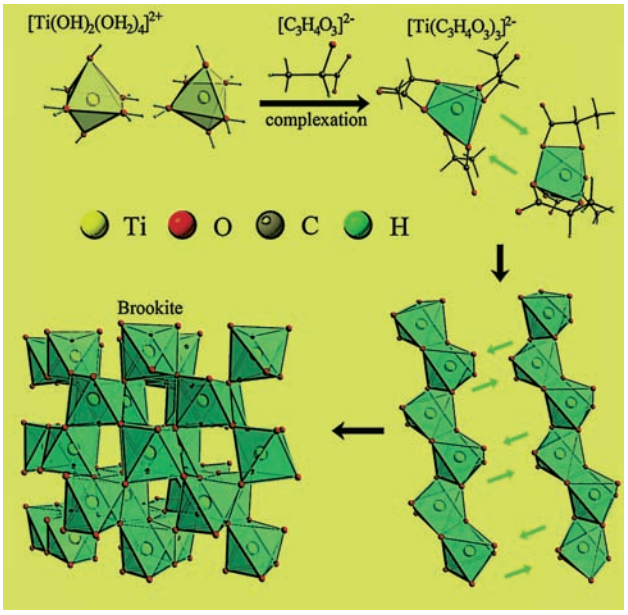

Figure 2. Formation mechanism proposed for phase-pure nanosheets of brookite TiO_2.

initial anatase structure progressively turned into brookite as a result of assimilation triggered by the primary brookite lattice in the presence of Na^+, as reported for other sodium-containing systems.[19] However, when sodium lactate was replaced by a mixture of lactic acid and NaCl during the preliminary 2 h of reaction, complexation of $[Ti(OH)_2(OH_2)_4]^{2+}$ by lactic acid to engender $[Ti(C_3H_4O_3)_3]^{2-}$ did not proceed effectively because the strong acidity of the reaction solution restrained the ionization of weak lactic acid. As a result, the subsequent course was mainly the dissociation of $[Ti(OH)_2(OH_2)_4]^{2+}$ to form a large quantity of anatase with little rutile and brookite (Figure S11b).

The present methodology is evidently characterized by a lower solution basicity (pH 8–9) resulting from the use of the hydrosoluble precursor $[Ti(C_3H_4O_3)_3]^{2-}$, which permits the successful preparation of high-quality brookite nanosheets with specific facets exposed (Figure 1) at a lower temperature (200 °C) for a shorter period of reaction (12 h). It should be mentioned that specific facets of brookite could not be successfully obtained under strongly basic (pH ≥10) or acidic (pH <2) solution conditions even at temperatures of ≥220 °C for reaction times of ≥20 h, as documented previously.[3,20] With these in mind, the exposure of specific facets is closely related to the absorption of extra lactate ions known as the surfactant onto the specific planes of brookite to reduce the surface energy,[21] thus causing the kinetically selective control of the growth rates of various faces of a grain seed. Consequently, brookite particles with well-developed facets were obtained.

The atomic structures of the exposed {210}, {201}, and {101} facets are illustrated in Figure 3a–c. From the stereo-shape model in Figure 3d, the percentages of these facets are estimated to be ~76, ~12, and ~12%, respectively. Previous theoretical calculations[22] have shown the sequence of surface energies of brookite TiO_2 to be 0.87 J/m^2 for {101} and 0.70 J/m^2 for {210}. Therefore, the {101} facets are expected to have

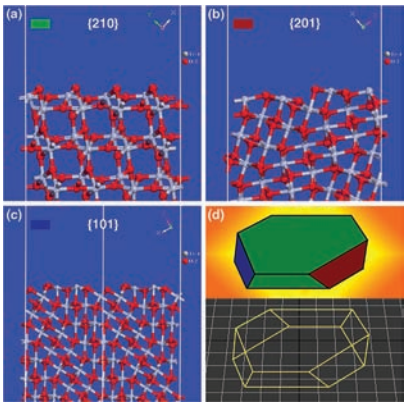

Figure 3. (a–c) Surface structures of brookite TiO_2: (a) {210}; (b) {201}; (c) {101} planes. (d) Stereo-shape model proposed for brookite nanosheets and its frame diagram.

a much higher reactivity than the common {210} facets because of the increased catalytically active sites on the highly energetic surfaces.[7] Another set of high-index {201} facets is barely accessible, although once they appear, they may show a catalytic activity superior to those of flat planes with atoms closely packed.[23] Furthermore, photodeposition of Pt and PbO_2 on brookite nanosheets was studied, following the methods reported in the literature for rutile and anatase.[24,25] It was found that the {201} facets serve as oxidation sites, while the remaining {210} and {101} facets act as reduction sites (Figure S8). Although the nanosheet thickness is small, the percentages of the {101} and {201} lateral facets are each as high as 12%, since these facets are not perpendicular to the basal planes. Therefore, brookite nanosheets are anticipated to be reactive in catalytic reactions by virtue of the exposure of high-energy {101} facets, and the photocatalytic efficiency can be evidently enhanced via trapping of the photoinduced holes and electrons by these redox sites,[9] which is of great interest.

The photocatalytic activity of brookite TiO_2 nanosheets was evaluated under UV irradiation using methyl orange (MO) as a probe molecule, as shown in Figure 4a. The relevant data for

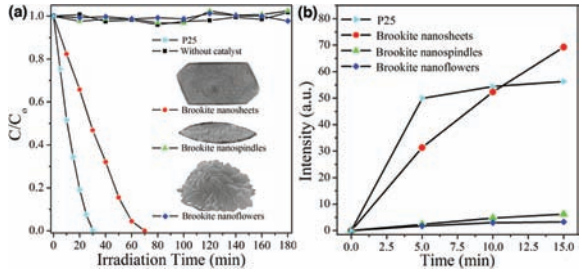

Figure 4. (a) MO photocatalytic degradation in the presence of brookite nanosheets, nanoflowers, and nanospindles, Degussa P25, and no catalyst. (b) Fluorescence intensities for these samples at 425 nm using terephthalic acid as a fluorescence probe of ·OH.

other morphologies surrounded with irregular surfaces (e.g., flower- and spindlelike brookite TiO_2) are also given for comparison. When no catalysts were involved, decomposition of MO was negligible within the test period of 3 h. Furthermore, flower- and spindlelike brookite did not show any catalytic activity toward MO decomposition. Comparatively, brookite nanosheets showed excellent activity in decolorization of MO with a complete degradation time of

dx.doi.org/10.1021/ja3014049 | J. Am. Chem. Soc. 2012, 134, 8328–8331

70 min. Increasing the preparation period of the nanosheets shortened the decomposition time by 10 min, indicating a catalytic activity superior to that of Degussa P25 in terms of unit specific surface area (Figure S9). Such an activity improvement could be ascribed to the evidently increased nanosheet thickness, which boosts the percentage of reactive {101} facets and oxidative {201} facets (Figures S4c, S4d).

The nature of the catalytic activity was further confirmed through ·OH measurements using terephthalic acid as a fluorescence probe under UV irradiation (Figure 4b and Figure S7). It was found that brookite nanospindles and nanoflowers showed a higher photoinduced electron−hole recombination rate, as represented by the faint fluorescence intensities. In contrast, the nanosheets showed a higher production rate of ·OH radicals relative to Degussa P25 TiO_2, which demonstrates an effective suppression of electron−hole recombination. The remarkable difference in activities for these morphologies could not derive from the surface areas, since the inert nanospindles have a surface area of 12.70 m^2/g, slightly smaller than that of 28.93 m^2/g for the highly active nanosheets (Table S1 in the SI). On the other hand, light-absorption discrepancies for these morphologies can be ignored under the present experimental conditions, as indicated by nearly the same absorption edges and band-gap energies (Figure S6). Therefore, the above experimental results testify that the photocatalytic property of brookite TiO_2 is highly dependent on its surface structure, and through exposure of high-energy {101} facets and effective separation of photoinduced electrons and holes for more ·OH radicals by these oxidative ({201}) and reductive ({210} and {101}) sites, one can tune this material from inert to highly reactive.

In summary, high-quality brookite TiO_2 nanosheets surrounded with four {210}, two {101}, and two {201} facets have been prepared using a novel low-basicity solution chemistry method. These nanosheets showed an outstanding activity toward degradation of organic contaminants that is even better than that of Degussa P25, while other morphologies such as irregularly faceted nanoflowers and nanospindles were catalytically inactive. These results indicate that the catalytic activity of brookite TiO_2 is highly morphology-dependent, which provides a new path for tuning the catalysts from inert to highly reactive. Furthermore, the facile synthesis and massive applications of pure brookite and explorations of the relationship between specific facets of brookite TiO_2 and their reactivities together with other related properties, which could not be realized in the past, are now feasible.

■ ASSOCIATED CONTENT

Supporting Information

Preparation, characterization, activity, ·OH measurements and Pt and PbO_2 photodeposition of brookite nanosheets, nanospindles, and nanoflowers; SEM and TEM images; UV−vis absorption, fluorescence, and Raman spectra; and specific surface areas and XRD patterns of the products obtained under conditions with distinct reaction periods and temperatures and various types of titanium sources and additives. This material is available free of charge via the Internet at http://pubs.acs.org.

■ AUTHOR INFORMATION

Corresponding Author

guangshe@fjirsm.ac.cn

Notes

The authors declare no competing financial interest.

■ ACKNOWLEDGMENTS

The authors acknowledge the financial support from the National Natural Science Foundation of China (21025104, 91022018, and 51072198) and the Important Scientific Problem Oriented Project of the Ministry of Science and Technology of China (2011CBA00501). The authors also express their thanks to Mr. Jing Zheng and Dr. Xiangfeng Guan for help in determining the crystal faces of the samples.

■ REFERENCES

(1) Diebold, U. *Surf. Sci. Rep.* **2003**, *48*, 53.
(2) Tong, H.; Ouyang, S. X.; Bi, Y. P.; Umezawa, N.; Oshikiri, M.; Ye, J. H. *Adv. Mater.* **2012**, *24*, 229.
(3) Deng, Q. X.; Wei, M. D.; Ding, X. K.; Jiang, L. L.; Ye, B. H.; Wei, K. M. *Chem. Commun.* **2008**, 3657.
(4) Li, G. H.; Gray, K. A. *Chem. Mater.* **2007**, *19*, 1143.
(5) Li, J.; Ishigaki, T.; Sun, D. *J. Phys. Chem. C* **2007**, *111*, 4969.
(6) Zhao, B.; Chen, F.; Huang, Q.; Zhang, J. *Chem. Commun.* **2009**, 5115.
(7) Bi, Y.; Ouyang, S.; Umezawa, N.; Cao, J.; Ye, J. *J. Am. Chem. Soc.* **2011**, *133*, 6490.
(8) Xie, X.; Li, Y.; Liu, Z. Q.; Haruta, M.; Shen, W. *Nature* **2009**, *458*, 746.
(9) Sun, L.; Qin, Y.; Cao, Q.; Hu, B.; Huang, Z.; Ye, L.; Tang, X. *Chem. Commun.* **2011**, *47*, 12628.
(10) Henderson, M. A. *Surf. Sci. Rep.* **2011**, *66*, 185.
(11) Koelsch, M.; Cassaignon, S.; Guillemoles, J. F.; Jolivet, J. R. *Thin Solid Films* **2002**, *403*, 312.
(12) Magne, C.; Dufour, F.; Labat, F.; Lancel, G.; Durupthy, O.; Cassaignon, S.; Pauporté, T. *J. Photochem. Photobiol., A* **2012**, *232*, 22.
(13) Hu, W.; Li, L.; Li, G.; Tang, C.; Sun, L. *Cryst. Growth Des.* **2009**, *9*, 3676.
(14) Tomita, K.; Petrykin, V.; Kobayashi, M.; Shiro, M.; Yoshimura, M.; Kakihana, M. *Angew. Chem., Int. Ed.* **2006**, *45*, 2378.
(15) Kandiel, T. A.; Feldhoff, A.; Robben, L.; Dillert, R.; Bahnemann, D. W. *Chem. Mater.* **2010**, *22*, 2050.
(16) Kakihana, M.; Tomita, K.; Petrykin, V.; Tada, M.; Sasaki, S.; Nakamura, Y. *Inorg. Chem.* **2004**, *43*, 4546.
(17) Nabivanets, B. I.; Kudritskaya, L. N. *Russ. J. Inorg. Chem.* **1967**, *12*, 616.
(18) Nabivanets, B. I.; Kudritskaya, L. N. *Russ. J. Inorg. Chem.* **1967**, *12*, 789.
(19) Buonsanti, R.; Grillo, V.; Carlino, E.; Giannini, C.; Kipp, T.; Cingolani, R.; Cozzoli, P. D. *J. Am. Chem. Soc.* **2008**, *130*, 11223.
(20) Pottier, A.; Chaneac, C.; Tronc, E.; Mazerolles, L.; Jolivet, J. P. *J. Mater. Chem.* **2001**, *11*, 1116.
(21) Ohno, Y.; Tomita, K.; Komatsubara, Y.; Taniguchi, T.; Katsumata, K.; Matsushita, N.; Kogure, T.; Okada, K. *Cryst. Growth Des.* **2011**, *11*, 4831.
(22) Gong, X.-Q.; Selloni, A. *Phys. Rev. B* **2007**, *76*, No. 235307.
(23) Tian, N.; Zhou, Z. Y.; Yu, N. F.; Wang, L. Y.; Sun, S. G. *J. Am. Chem. Soc.* **2010**, *132*, 7580.
(24) Ohno, T.; Sarukawa, K.; Matsumura, M. *New J. Chem.* **2002**, *26*, 1167.
(25) Bae, E.; Ohno, T. *Appl. Catal., B* **2009**, *91*, 634.